THE JOURNAL OF PHYSICAL CHEMISTRY LETTERS
A JOURNAL OF THE AMERICAN CHEMICAL SOCIETY

pubs.acs.org/JPCL Letter

Water Cages as Chemical Reactors: VUV Photolysis of Dimethyl Ether Clathrate Hydrate Thin Films in Ultrahigh Vacuum

Bijesh K. Malla, Soham Chowdhury, Khushboo Bhardwaj, Rajnish Kumar,* and Thalappil Pradeep*

Cite This: https://doi.org/10.1021/acs.jpclett.6c00029 Read Online

ACCESS | Metrics & More | Article Recommendations | Supporting Information

ABSTRACT: Clathrate hydrates (CHs) are crystalline molecular solids with hydrogen-bonded water cages where small molecules are trapped and are important in both terrestrial and extraterrestrial environments. While the structural stability and phase behavior of CHs and related ices are well characterized, key questions about their role as reactive environments under energetic radiation remain unanswered. Here, we show that dimethyl ether (DME) CH thin films in ultrahigh vacuum ($\sim 10^{-10}$ mbar) can be switched from passive ice cages into active chemical reactors under vacuum-ultraviolet (VUV) photolysis at cryogenic temperatures (10−130 K). Temperature-dependent irradiation reveals that at 10 K, VUV photolysis leads to rapid dissociation of the DME CH, dissociation of the cage framework, and formation of amorphous ice with no efficient trapping of photoproducts. In contrast, at 130 K the hydrate cages partially reform during or after photolysis, and photoproduced formaldehyde (H_2CO) becomes confined within the reformed cages, enabled by increased intermolecular mobility. A comparison of DME dissociation and CH_4 photoproduction in pure DME ice, DME−water amorphous ice mixtures, and DME CH at 10 K shows that CH_4 formation and DME dissociation rate are highest for the clathrate phase, indicating the cage effect where the interaction of DME and water is minimal even in the condensed phase. These findings demonstrate that CH cages can act as VUV-driven chemical nanoreactors in the condensed phase, providing a mechanistic link between ice cage structure, photolytic dissociation, and the formation of reactive products under space-relevant conditions.

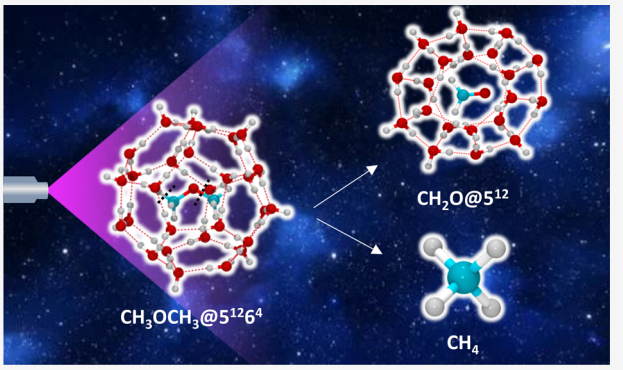

The growth of clathrate hydrates (CHs) within amorphous ice mixtures of water and guest molecules has been well-established by infrared spectroscopy and electron diffraction techniques under ultrahigh vacuum (UHV) and cryogenic conditions, mimicking interstellar environments.[1−4] An early study was reported under high-vacuum conditions.[5] CHs are crystalline compounds where water molecules form hydrogen-bonded cages to encapsulate small guest molecules such as CO_2, CH_4, C_2H_6, and O_2,[6−11] and they form typically under high-pressure, low-temperature (near 0 °C) conditions.[12−17] Recent studies have shown that even under UHV conditions, around 130 K, CH formation becomes more efficient when guest molecules can form hydrogen bonds.[18−20] Furthermore, these conditions facilitate the nucleation of CHs with small molecules, such as CO_2, and N_2O.[21,22]

Several characterization tools, including infrared spectroscopy, electron diffraction, and X-ray diffraction, have been used to detect the formation of CHs within a vacuum range of 10^{-6} to 10^{-10} mbar.[5,23−25] Interestingly, many molecules form metastable CHs in vacuum environments, which can transform into hexagonal or cubic ice upon heating.[26−28] The presence of CHs has also been suggested in space environments, such as on comets and in protostellar systems.[5] Given the exposure to energetic radiation in space, it is crucial to understand the stability and transformation of CHs under these conditions.

While the formation and transformation of CHs under high-pressure and vacuum conditions have been explored, there has been limited focus on their behavior under energetic radiation. Michon et al. demonstrated the two-photon photolysis of tetrahydrofuran (THF) in CH cages at 77 K, detecting short-lived organic radicals using electron spin resonance spectroscopy.[29] Ahn et al.[30] reported lattice expansion in CHs due to gamma ray irradiation. Additionally, interactions of low-energy electrons and photons with cage-like molecular systems have been examined in UHV, though these have not been explicitly attributed to CHs.[31−33] Despite these efforts, the photochemistry of CHs under condensed-phase, interstellar-like conditions remains unexplored. The present work investigates

Received: January 6, 2026
Revised: February 28, 2026
Accepted: March 4, 2026

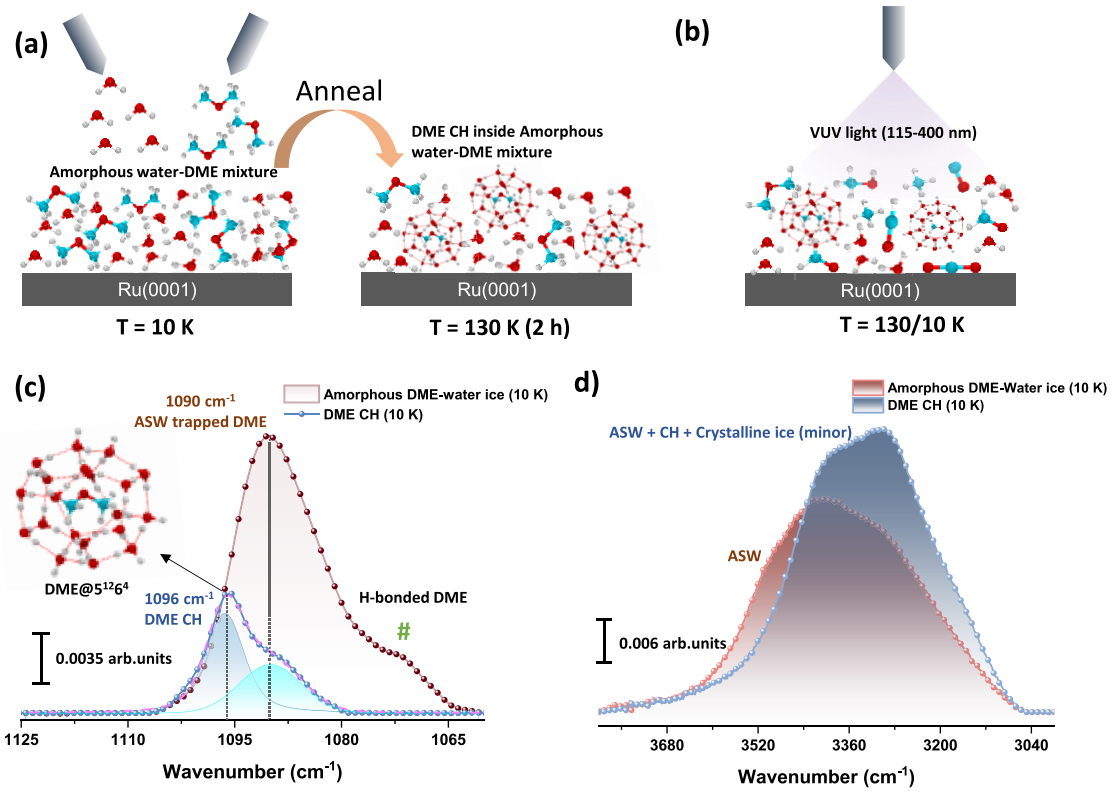

Figure 1. Formation of DME CH was studied by RAIRS. (a) Schematic of the formation of DME CH, amorphous DME-water ice mixture created by vapor deposition on Ru(0001) for 10 K followed by annealing at 130 K for 2 h. (b) Schematic of the VUV photoirradiation of DME CH at 10 and 130 K. (c) RAIR spectra of amorphous DME-water ice mixture and DME CH in the C-O antisymmetric stretching region at 10 K. RAIR spectrum of DME CH is deconvoluted into two peaks, and highlighted in blue (1096 cm^{-1}) and cyan (1090 cm^{-1}) colors. The broad peak shown by the symbol # represents the H-bonded DME molecules. (d) RAIR spectra of amorphous DME-water ice mixture and DME CH in the O-H stretching region at 10 K.

the vacuum ultraviolet photolysis of dimethyl ether (DME) CHs at 10 and 130 K, comparing the dissociation dynamics of CH cages and DME molecules. Remarkably, at 130 K, photoproduced formaldehyde reincorporates into CH cages, while at 10 K, it remains in an amorphous state. Furthermore, the dissociation rate of DME and the photoproduction rate of CH_4 are significantly higher in the CH phase than in pure DME ice or DME−water ice mixtures. Interactions between DME molecules and their surrounding DME and water neighbors play a crucial role in governing DME dissociation and CH_4 formation across the three different phases. Additionally, differences in molecular mobility at low temperatures (10 and 130 K) significantly influence cage disruption and the confinement of formaldehyde within the clathrate structure.

All experiments were conducted in a custom-built UHV instrument with a base pressure of ~5 × 10^{-10} mbar. A highly polished Ru(0001) single crystal was used as the substrate to create thin ice films, which was mounted on a copper holder. It was connected to a helium cryostat (Cold Edge technology), which could maintain a temperature as low as 8 K. A resistive heater (25 Ω), controlled by a temperature controller (Lakeshore 336), was used to heat the substrate to 1000 K The RAIRS data was collected in the 4000−550 cm^{-1} range with a spectral resolution of 2 cm^{-1}, using a Bruker FT-IR spectrometer, Vertex 70. The ice sample was exposed to an incident angle of 80 ± 7° by focusing the IR beam through a ZnSe viewport. The reflected IR beam from the sample was detected using a liquid N_2-cooled mercury cadmium telluride (MCT) detector. An Extrel quadrupole mass spectrometer was used for TPD-MS in an out-of-sight configuration. A deuterium lamp (McPherson, Model 634, with MgF_2 window, 30 W) of vacuum ultraviolet (VUV) range 115−400 nm was used as the UV light source. The VUV lamp was differentially pumped and attached to the UHV chamber through the MgF_2 window (with a cutoff at ~ 114 nm (10.87 eV)). A detailed description of the experimental part is provided in the Supporting Information.

Formation of DME CH

Clathrate hydrate (CH) of DME was prepared by thermally annealing a vapor-deposited DME-water ice mixture with a 1:5 ratio to 130 K and maintaining this temperature for 2 h, as shown in Figure 1a. After the CH formation, the system was cooled back to 10 K, and an IR spectrum was recorded. Figure 1c,d shows the RAIR spectra of the DME-water amorphous ice mixture and the DME CH at 10 K in the C−O antisymmetric stretching region of DME and the O−H stretching region of water, respectively. In the DME-water amorphous ice mixture, the peak at 1090 cm^{-1} corresponds to DME trapped in amorphous solid water (ASW), while the peak marked # indicates hydrogen-bonded DME with water molecules. After CH formation, this peak (#) disappears, signifying the loss of hydrogen-bonding character, which has been discussed in detail in our previous study.[20] The emergence of a peak at 1096 cm^{-1} indicates the formation of sII CH of DME, where 61% of DME was found to be incorporated into $5^{12}6^4$ cages, while 29% remained trapped in ASW. A detailed discussion

https://doi.org/10.1021/acs.jpclett.6c00029
J. Phys. Chem. Lett. XXXX, XXX, XXX−XXX

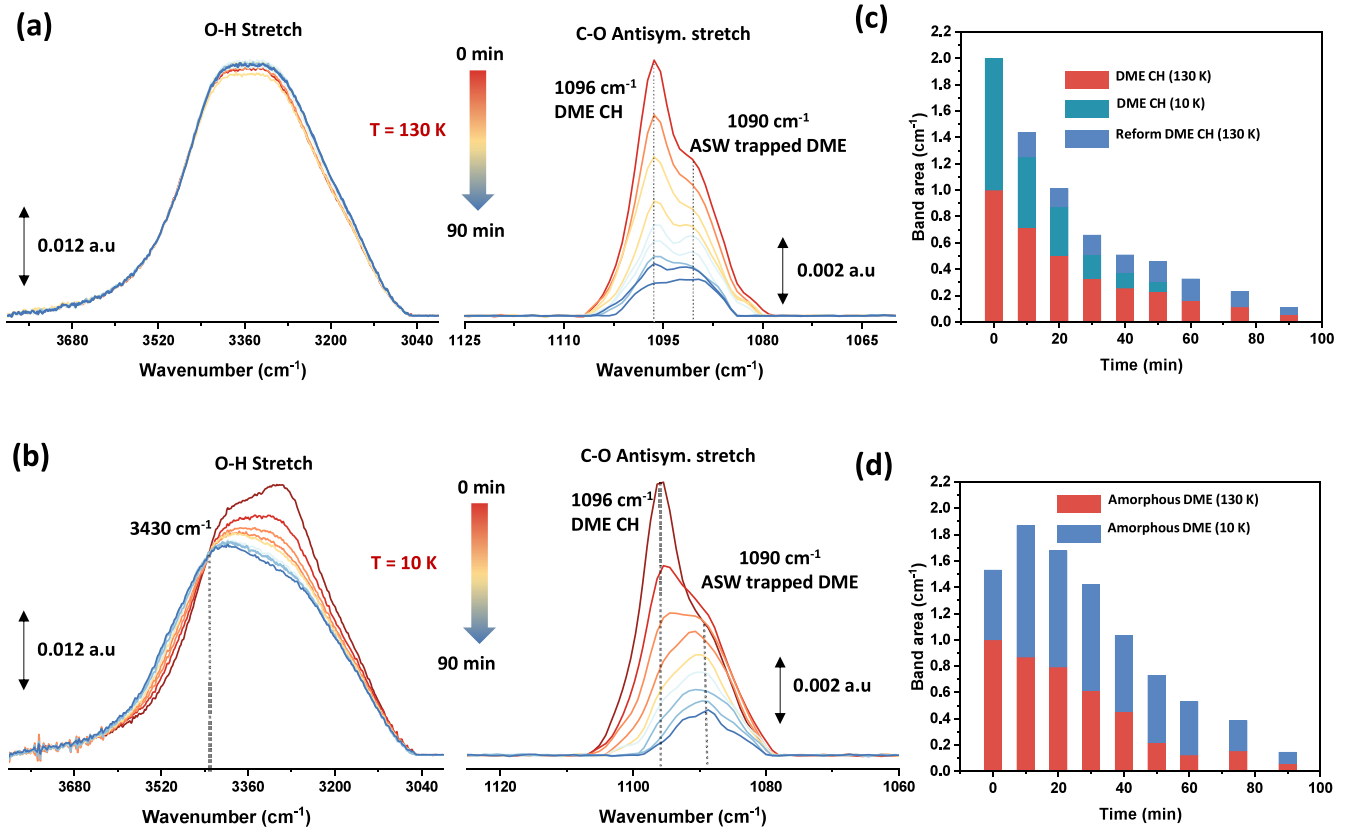

Figure 2. RAIRS study of the dissociation of sII DME CH. Time-dependent RAIR spectra of photoirradiated DME CH in the (a) O−H stretching region and in the C−O antisymmetric stretching region, at 130 K (b). Time-dependent RAIR spectra of photoirradiated DME CH in the O−H stretching region and in the C−O antisymmetric stretching region at 10 K. Each spectrum of (b) and (d) in the C−O antisymmetric stretch is deconvoluted into two peaks at 1096 cm^{-1} (DME CH) and 1090 cm^{-1} (ASW trapped DME) and the band area is calculated. (d) Deconvoluted band area of ASW trapped DME at 130 and 10 K with respect to irradiation time. (c) Deconvoluted band area of DME CH at130 and 10 K with respect to irradiation time. "Reform DME CH" was calculated by subtracting the band area of DME CH from 130 to 10 K.

about the cage assignment is provided in our earlier studies with suitable references. Additionally, Figure 1d shows the RAIR spectra in the O−H stretching region, where a broad peak indicates amorphous nature of water-ice. Upon CH formation, this broad peak narrowed, indicating the ordering of water molecules due to the formation of DME CH. Furthermore, a fraction of crystalline ice might be present in the ice matrix as we have waited at 130 K for 2 h. We note here that, as RAIRS shows the bulk property of a thin film, and not all the DME is converted to CH, there are three types of water-ice, namely ASW, crystalline ice, and CH present in the ice matrix.

Photolysis of DME and DME-H_2O Ice

Before exploring the photochemistry of DME CH, we first focused on the photochemistry of pure DME and a DME-water mixture. Understanding the photochemical behavior in the absence and presence of water is essential for comparison. Following 90 min of irradiation of pure DME, two new peaks at 3005 cm^{-1} and 1304 cm^{-1} arose, corresponding to the C−H antisymmetric and asymmetric bending mode of methane (CH_4) (Figure S1).[34] The presence of carbon monoxide (CO) was detected by a peak at 2135 cm^{-1}, attributed to the C≡O stretching mode. Formaldehyde (HCHO) was identified by a peak at 1722 cm^{-1}, characteristic of the C═O antisymmetric stretching. Additionally, methanol (CH_3OH) and ozone (O_3) were both associated with a broad peak at 1043 cm^{-1}, which can be attributed to a combination of the C−O antisymmetric stretch of methanol and the O−O stretching mode of ozone (Figure S1).[35] All photoproducts were further confirmed by reactive ion scattering (RIS) experiments (experimental details are provided in the Supporting Information). In RIS, Cs^+ ions form ionic clusters with neutral molecular species present on the ice surface. The observed mass peaks originate from Cs^+ adducts of neutral molecules on the ice surface, allowing for the unambiguous identification of the photoproducts (Figure S2). We note that the relative intensity of photoproducts in the RIS mass spectrum does not reflect their actual relative concentrations in the bulk. This is because RIS probes only the surface composition, and the abstraction reaction is driven by the ion−dipole attraction between the Cs^+ ion and a surface species. Those with higher dipole moments exhibit more efficient pickup, which results in their higher intensities in the mass spectrum. Furthermore, we have done TPD-MS study of photoirradiated DME. After 90 min of irradiation, we have annealed the sample to 200 K with an annealing rate of 10 K/min and collected a mass spectrum giving m/z 45 ($CH_3OCH_2^+$), 16 (CH_4^+), 30 (CH_2O^+), and 31 (CH_3O^+) (Figure S3). These 4 major peaks arise from fragments or intact ions of DME, methane, formaldehyde, and methanol. The mass spectrum shows a peak at 97 K, which is the desorption peak for the pure DME. Here, it is worth noting that all the photoproducts are desorbed, along with the desorption of DME. Interestingly, in the case of methane, a hump was observed in the spectrum from 60 to 80 K. This

https://doi.org/10.1021/acs.jpclett.6c00029
J. Phys. Chem. Lett. XXXX, XXX, XXX−XXX

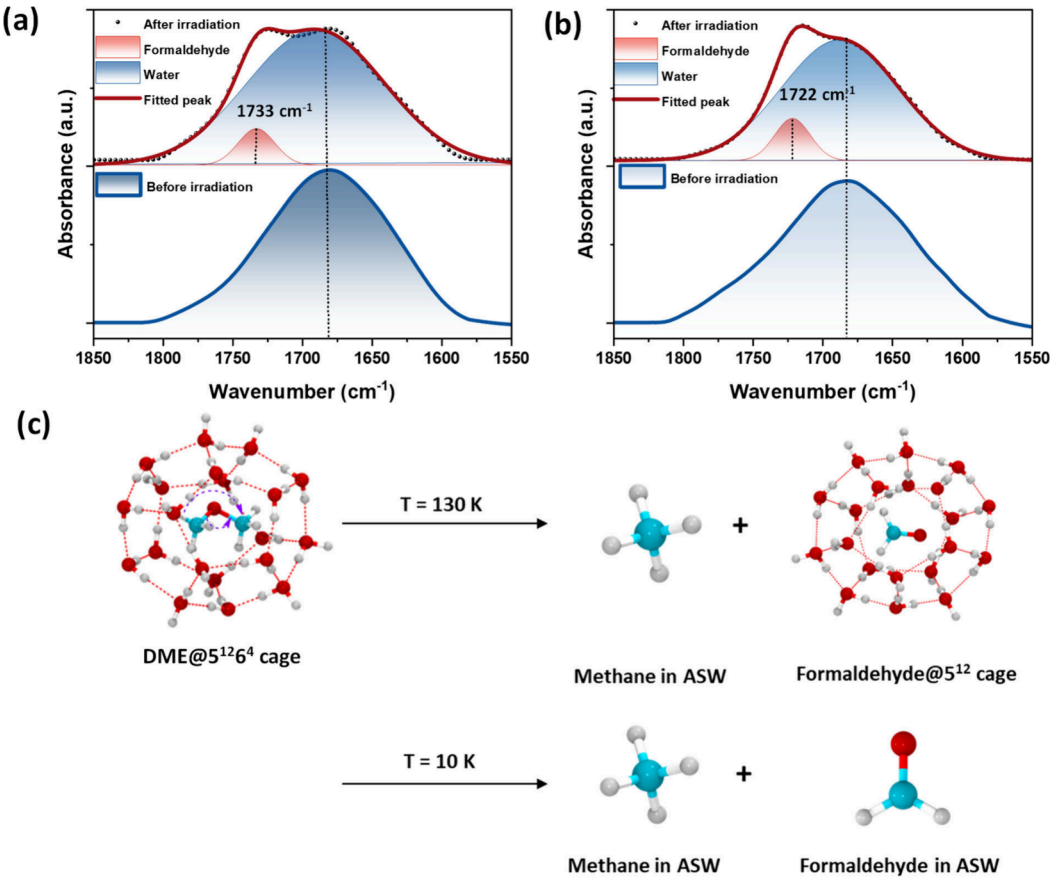

Figure 3. RAIR spectra of DME CH before and after 90 min irradiation, in the O−H bending region in (a) at 130 K, in (b) at 10 K. In both (a) and (b) after irradiation the spectrum is deconvoluted into two components, shown in red shade (representing formaldehyde, in C═O stretching region) and in blue shade (representing water). (c) Schematic of DME photochemistry in CH at two temperatures and the corresponding photoproducts in distinct ice forms.

feature is attributable to partial diffusion of methane to the surface after desorption. For comparison, we have provided the gas-phase electron−ionization mass spectrum of DME in Figure S4, in which the proposed photoproducts, methane and formaldehyde, are absent. Additionally, we irradiated 300 ML of DME-water ice mixture for 90 min and collected IR spectra (Figure S5). The same photoproducts were observed as in pure DME ice. A high-intensity peak observed at 1043 cm^{-1} is attributed to the increased concentration of methanol, formed via the reaction between H_2O and DME.

Photolysis of DME CH

The phototransformation of DME was studied at two distinct temperatures: 10 and 130 K (Figure 1d), with the corresponding RAIR spectra in the O−H stretching region of H_2O and the C−O antisymmetric stretching. stretching region of DME, presented in Figure 2. The choice of these temperatures was motivated by the role of thermal activation in modulating the intermolecular mobility of DME and H_2O within the CH structure. At 130 K, enhanced mobility allowed the reformation and reorganization of CH cages.[36] In contrast, at 10 K, the limited molecular motion prevented such rearrangements, leading to rapid cage dissociation. DME exists in two different environments within the ice matrix, as indicated by distinct peak positions in the RAIR spectrum: 1096 cm^{-1} corresponding to DME within the $5^{12}6^4$ cage structure and 1090 cm^{-1} attributed to DME trapped in ASW.[20] The extent of CH cage deformation is monitored by the decrease in the 1096 cm^{-1} peak intensity. During the first 60 min of VUV irradiation, spectra were recorded every 10 min, followed by additional spectra at 15 min intervals until 90 min. Figure 2a,b shows the time-dependent evolution of the O−H stretching and C−O antisymmetric stretching bands of DME CH under VUV irradiation at both 130 and 10 K. At 10 K, the intensity of the 1096 cm^{-1} band decreased significantly faster than at 130 K. The normalized band areas at both temperatures are compared in Figure 2c,d. After 50 min of irradiation at 10 K, the 1096 cm^{-1} band completely vanished (Figure 2b), indicating the complete destruction of CH cages. In contrast, at 130 K, the 1096 cm^{-1} band persisted for up to 90 min, indicating slower cage dissociation and partial reformation (Figure 2a). To quantify this reformation, the difference in the band area of the 1096 cm^{-1} peak at 130 and 10 K was calculated and defined as "reformed hydrate", highlighting that thermal energy at 130 K promotes the reformation of CH cages (Figure 2c). The 1090 cm^{-1} band, associated with ASW-trapped DME, showed a slower decline at 10 K compared to 130 K, as shown in Figure 2d. This behavior can be attributed to two factors: (i) faster uncaged DME dissociation in the ASW matrix at 130 K, and (ii) the lack of CH reformation at 10 K. Time-dependent RAIR spectra in the O−H stretching region (Figure 2a,b) further confirm these observations. At 10 K, a phase transition from crystalline to amorphous ice was observed, indicated by the broadening of the O−H stretching band (Figure 2b). However, at 130 K, no significant changes were observed, suggesting that thermal

https://doi.org/10.1021/acs.jpclett.6c00029
J. Phys. Chem. Lett. XXXX, XXX, XXX−XXX

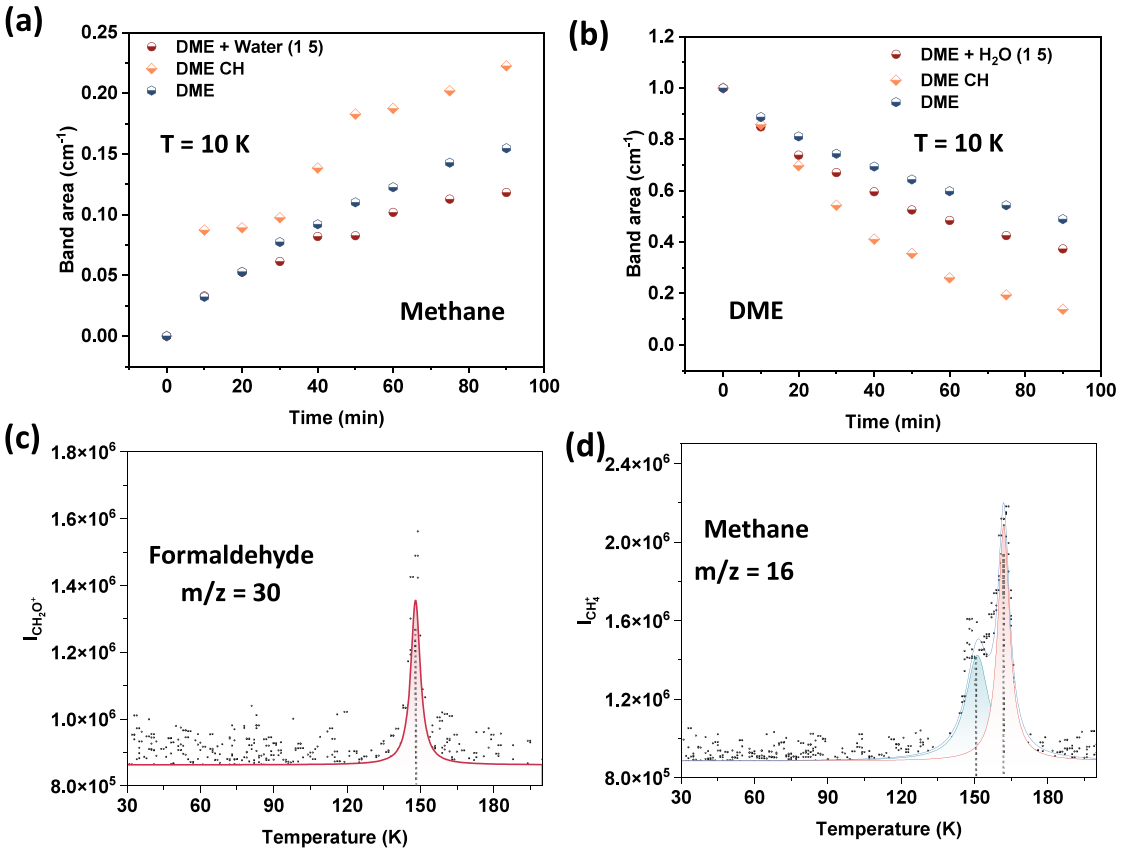

Figure 4. (a) Comparison of the evolution of band area of methane formed during the photolysis of pure DME, DME + water, and DME CH as a function of time. (b) Comparison of the band area evolution of DME during the photolysis of pure DME, DME + water, and DME clathrate CH as a function of time. TPD-MS spectrum of photoirradiated deuterated DME CH (CH_3OCH_3+D_2O). Integrated ion counts of (c) m/z 30 and (d) m/z 16 are plotted as a function of temperature.

annealing at this temperature provides sufficient energy for the reformation of CH cages. Here, we conclude that continuous thermal annealing at 130 K supplies the necessary energy to promote the reformation of CH cages, a process that is hindered at 10 K due to the lack of thermal energy. This observation raises a critical question of the role of reformation of CH cages in capturing and stabilizing the photoproduced molecules formed during VUV irradiation.

From the photochemistry of pure DME and DME-water ice, formaldehyde and methane emerged as the two primary photoproducts.[35,37−39] Methane, being a smaller molecule, becomes highly mobile at 130 K, allowing it either to escape from the system or become trapped in the pores of amorphous ice. Therefore, we exclude the potential effect of CH cages on methane stability and confinement. Figure 3a,b displays the infrared absorption bands of formaldehyde in C═O stretching region at 130 and 10 K, respectively. After 90 min of irradiation at 10 K, formaldehyde exhibited a peak at 1722 cm^{-1}, whereas, under the same irradiation time at 130 K, a distinct blue-shifted peak at 1733 cm^{-1} was observed, an 11 cm^{-1} shift from the 10 K peak. Ghosh et al.[40] assigned the peak at 1733 cm^{-1} as formaldehyde confined within CH cages, while the 1722 cm^{-1} peak corresponded to amorphous formaldehyde, characteristic of its unconfined state at low temperatures. In agreement, we observed the same peak at 1722 cm^{-1} for formaldehyde when DME was irradiated at 10 K, which indicated amorphous formaldehyde. At 130 K, however, the 1733 cm^{-1} peak suggests that the thermal energy is sufficient to drive the reformation of CH cages, thus enabling the confinement of formaldehyde within a cage environment, likely to be affected by the UV irradiation. In contrast, at 10 K, the lack of thermal energy prevents the reformation of CH cages, leaving the newly formed formaldehyde in an amorphous state within the ice matrix. To further substantiate this assignment and quantitatively evaluate the peak positions, we performed an additional spectral deconvolution analysis. The postirradiation spectra at 10 and 130 K were each fitted three times, considering three different possible shoulder contributions for formaldehyde. For the 130 K spectra, peak centers at 1733, 1728, and 1738 cm^{-1} were tested, whereas for the 10 K spectra, peak centers at 1722, 1717, and 1727 cm^{-1} were evaluated (Figure S6). The results clearly demonstrate that the best fits are obtained with peak centers at 1733 cm^{-1} for 130 K and 1722 cm^{-1} for 10 K."

We have also tracked the methane formation in these two temperatures, at 10 K, the emerging peak at 1304 cm^{-1} suggests that methane is in the amorphous form. Schriver et al. reported that formaldehyde and CH_4 are the primary products of DME photodissociation via C−O and C−H bond cleavage (Figure 3c).[38] In the present CH system, we propose that DME undergoes self-dissociation within the clathrate cages, producing formaldehyde and CH_4 with minimal involvement of water molecules. This interpretation is further supported by experiments using a D_2O ice system, as discussed in a later section. Subsequently, we focused on whether the

https://doi.org/10.1021/acs.jpclett.6c00029
J. Phys. Chem. Lett. XXXX, XXX, XXX−XXX

CH cage environment modulates DME dissociation and subsequent photoproduct formation.

DME dissociates into formaldehyde and methane when confined inside large hydrate cages ($5^{12}6^4$), exhibiting gas-phase-like behavior due to minimal interactions with the surrounding cage molecules, leading to potentially faster dissociation. It is well established that the absorption of VUV photons by pure ASW is very low, as we confirmed by irradiating ASW for 6 h without observing any significant spectral changes in the mid-infrared region.[41,42] However, the presence of a foreign molecule within ASW could influence photoreactivity.[43−46] To validate this, we examined three cases: pure DME, a DME-water ice mixture, and DME CH, irradiating all three systems at 10 K. Methane, identified as our primary photoproduct, was quantified by calculating the peak area for the ν_4 band at 1304 cm^{-1}.[47] DME CH irradiated at 130 K was not considered due to the potential desorption of methane from the matrix at this temperature (Figure S7b). The C−O antisymmetric stretching mode of DME in all three systems was normalized to 1 before irradiation, and all methane band areas were subsequently normalized to their respective DME (reactant) band areas. Figure 4a compares methane production from amorphous DME-water ice, DME CH, and pure DME (Figure S8a−c). Methane production was significantly higher in DME CH than in pure DME or the DME-water mixture. In pure DME, there appears to be a molecular hindrance between DME molecules, and in the DME-water mixture, strong hydrogen bonding interactions occur between water and DME molecules. In contrast, within DME CH, DME remains as isolated molecules, behaving more like free molecules and resulting in a higher yield of photoproducts. As previously discussed, at 10 K, the hydrate cages break after 50 min of irradiation. This trend is reflected in Figure 4a, where methane production is rapid up to 50 min, followed by a slower increase. Comparing pure DME with the DME-water system, the photoproduct yield is considerably higher in pure DME, attributed to the absence of hydrogen bonding in the pure system. In the DME-water system, water introduces hydrogen bonding, reducing the reaction efficiency. The dissociation rate of DME was tracked for all three systems (Figure 4b). The highest dissociation rate is observed in the CH system, followed by the DME−water mixture, and then pure DME (Figure S8d−f). The faster dissociation in the CH system can be attributed to reduced steric hindrance for DME within the clathrate cages. The enhanced dissociation of DME in the DME−water system compared to pure DME is likely due to increased photoproduct formation arising from interactions with water molecules. Notably, this photoproduct is not methane, as indicated by the trend in Figure 4a; instead, other byproducts, such as methanol, dominate. Since RAIR spectroscopy primarily guided this study, mass spectrometry was employed for additional insights. We created deuterated DME CH by codepositing D_2O and DME, followed by annealing at 135 K for 2 h and subsequent cooling to 10 K. Figure S9 shows the RAIR spectra of deuterated DME CHs in the C−O antisymmetric stretching and O−D symmetric stretching regions. The system was irradiated for 90 min using the same irradiation protocol as applied to the previous experiments, after which temperature-dependent mass spectra were recorded. Following irradiation, the broad O−D stretching band indicates the amorphous nature of the water ice (Figure S10c,d). Two m/z values, 30 (HCHO) and 16 (CH_4), corresponding to formaldehyde and methane, were selected (Figure 4c,d). A desorption peak for formaldehyde was observed at 149 K, while methane showed two peaks at 151 and 161 K, indicating minimal interference from deuterium atoms in D_2O ice. These results support the conclusion that both methane and formaldehyde are formed predominantly via photodissociation of DME within the clathrate cages, rather than through secondary reactions involving the surrounding water matrix. Additionally, two photoirradiation experiments were performed on deuterated (D_2O) DME CHs at 135 and 10 K. The dissociation dynamics closely match those observed for DME CHs prepared with H_2O ice. Figure S10 presents the corresponding RAIR spectra in the C−O antisymmetric stretching and O−D stretching regions. These results further demonstrate the reproducibility and consistency of the experimental observations. Together, these experiments demonstrate how the transition from amorphous ice to clathrate "ice cages" fundamentally alter the photochemical behavior of DME under VUV irradiation.

We have investigated the VUV-induced photodissociation of DME CH thin films in ultrahigh vacuum, revealing how temperature controls the transition from passive ice cages to active chemical reactors. Photolysis experiments at 10 and 130 K exhibit distinct behaviors: at 10 K, rapid disruption of the clathrate cages leads to collapse of the hydrate framework into an amorphous ice matrix, in which photoproducts are not efficiently confined. In contrast, at 130 K, the increased thermal energy enables partial reformation of the clathrate cages, allowing DME to remain encapsulated, providing a confined environment for subsequent chemistry. Under these conditions, photoproduced formaldehyde is trapped within the reformed cages, whereas at 10 K it remains as an amorphous deposit in the ice. Our results further show that DME dissociation is significantly more efficient in the CH phase than in pure DME ice or amorphous DME−water mixtures, yielding the highest methane production in the clathrate system. Complementary TPD−MS measurements indicate that methane and formaldehyde originate predominantly from the self-dissociation of cage-confined DME and are largely independent of direct reactions with bulk water. Taken together, these findings demonstrate that DME CHs can act as VUV-driven chemical nanoreactors under space-relevant conditions, providing critical insight into the photochemical pathways of guest molecules in clathrate-rich astrochemical environments.

■ ASSOCIATED CONTENT

Supporting Information

The Supporting Information is available free of charge at https://pubs.acs.org/doi/10.1021/acs.jpclett.6c00029.

Experimental section (including experimental setup, materials and reagents, and sample preparation) and temperature and time-dependent RAIR spectra (PDF)
Transparent Peer Review report available (PDF)

■ AUTHOR INFORMATION

Corresponding Authors

Rajnish Kumar − *Department of Chemical Engineering and School of Sustainability, Indian Institute of Technology Madras, Chennai 600036, India;* orcid.org/0000-0002-4172-2638; Email: rajnish@iitm.ac.in

Thalappil Pradeep − *DST Unit of Nanoscience (DST UNS) and Thematic Unit of Excellence (TUE), Department of Chemistry, Indian Institute of Technology Madras, Chennai*

https://doi.org/10.1021/acs.jpclett.6c00029
J. Phys. Chem. Lett. XXXX, XXX, XXX−XXX

600036, India; International Centre for Clean Water, IIT Madras Research Park, Chennai 600113, India; orcid.org/0000-0003-3174-534X; Email: pradeep@iitm.ac.in

Authors

Bijesh K. Malla − *DST Unit of Nanoscience (DST UNS) and Thematic Unit of Excellence (TUE), Department of Chemistry, Indian Institute of Technology Madras, Chennai 600036, India; Department of Chemical Engineering, Indian Institute of Technology Madras, Chennai 600036, India;* orcid.org/0009-0005-1148-0884

Soham Chowdhury − *DST Unit of Nanoscience (DST UNS) and Thematic Unit of Excellence (TUE), Department of Chemistry, Indian Institute of Technology Madras, Chennai 600036, India;* orcid.org/0009-0000-8151-6065

Khushboo Bhardwaj − *Department of Chemistry, Indian Institute of Technology Madras, Chennai 600036, India*

Complete contact information is available at: https://pubs.acs.org/10.1021/acs.jpclett.6c00029

Author Contributions

B.K.M. designed the experiments. B.K.M. and S.C. performed the experiments. B.K.M., S.C., and K.B. analyzed the results. T.P. and R.K. supervised the progress. B.K.M. wrote the first draft of the manuscript. The final version of the manuscript was prepared, including the contributions of all authors.

Notes

The authors declare no competing financial interest.

■ ACKNOWLEDGMENTS

We acknowledge the Science and Engineering Research Board (SERB), Department of Science and Technology (DST), and Government of India for research funding. T.P. acknowledges funding from the Centre of Excellence (CoE) on Molecular Materials and Functions under the Institution of Eminence scheme of IIT Madras. S.C. thanks IITM for their research fellowship. We thanks Dr. Sharma S. R. K. C. Yamijala for helpful discussions.

■ REFERENCES

(1) Ghosh, J.; Methikkalam, R. R. J.; Bhuin, R. G.; Ragupathy, G.; Choudhary, N.; Kumar, R.; Pradeep, T. Clathrate Hydrates in Interstellar Environment. *Proc. Natl. Acad. Sci.* **2019**, *116* (5), 1526−1531.

(2) Tychengulova, A.; Katpayeva, K.; Shomshekova, S.; Ibragimova, S.; Golikov, O.; Yerezhep, D.; Sokolov, D.; Aldiyarov, A. Laboratory Studies of the Clathrate Hydrate Formation in the Carbon Dioxide-Water Mixtures at Interstellar Conditions. *ACS Omega* **2025**, *10* (1), 1237−1248.

(3) Ghosh, J.; Vishwakarma, G.; Kumar, R.; Pradeep, T. Formation and Transformation of Clathrate Hydrates under Interstellar Conditions. *Acc. Chem. Res.* **2023**, *56* (16), 2241−2252.

(4) Malla, B. K.; Yang, D.-S.; Pradeep, T. Growth of Clathrate Hydrates in Nanoscale Ice Films Observed Using Electron Diffraction and Infrared Spectroscopy. *J. Phys. Chem. Lett.* **2025**, *16* (1), 365−371.

(5) Blake, D.; Allamandola, L.; Sandford, S.; Hudgins, D.; Freund, F. Clathrate Hydrate Formation in Amorphous Cometary Ice Analogs in Vacuo. *Science (80).* **1991**, *254* (5031), 548−551.

(6) Sloan, E. D., Jr.; Koh, C. A. Introduction: Clathrate Hydrates of Natural Gases. *Clathrate Hydrates Nat. Gases* **2007**, I−XXV.

(7) Kuhs, W. F.; Hansen, T. C.; Falenty, A. Filling Ices with Helium and the Formation of Helium Clathrate Hydrate. *J. Phys. Chem. Lett.* **2018**, *9* (12), 3194−3198.

(8) Nguyen, A. H.; Molinero, V. Cross-Nucleation between Clathrate Hydrate Polymorphs: Assessing the Role of Stability, Growth Rate, and Structure Matching. *J. Chem. Phys.* **2014**, *140* (8), 084506.

(9) Yeon, S. H.; Seol, J.; Lee, H. Structure Transition and Swapping Pattern of Clathrate Hydrates Driven by External Guest Molecules. *J. Am. Chem. Soc.* **2006**, *128* (38), 12388−12389.

(10) Cui, J.; Sun, Z.; Wang, X.; Yu, B.; Leng, S.; Chen, G.; Sun, C. Fundamental Mechanisms and Phenomena of Clathrate Hydrate Nucleation. *Chin. J. Chem. Eng.* **2019**, *27* (9), 2014−2025.

(11) Makogon, Y. F. Natural Gas Hydrates - A Promising Source of Energy. *J. Nat. Gas Sci. Eng.* **2010**, *2* (1), 49−59.

(12) Kumar, A.; Daraboina, N.; Linga, P.; Kumar, R.; Ripmeester, J. A. Experimental Study on Hydrate Structure Transition Using an In Situ High-Pressure Powder X-Ray Diffractometer: Application in CO2 Capture. *ACS Sustain. Chem. Eng.* **2022**, *10* (35), 11473−11482.

(13) Bhattacharjee, G.; Prakash Veluswamy, H.; Kumar, R.; Linga, P. Rapid Methane Storage via SII Hydrates at Ambient Temperature. *Appl. Energy* **2020**, *269*, 115142.

(14) Takeya, S.; Hachikubo, A. Crystal Structure and Guest Distribution of N_2O Hydrate Determined by Powder X-Ray Diffraction Measurements. *Cryst. Growth Des.* **2022**, *22* (2), 1345−1351.

(15) Takeya, S.; Fujihisa, H.; Hachikubo, A.; Sakagami, H.; Gotoh, Y. Distribution of Butane in the Host Water Cage of Structure II Clathrate Hydrates. *Chem. Eur. J.* **2014**, *20*, 17207−17213.

(16) Khurana, M.; Yin, Z.; Linga, P. A Review of Clathrate Hydrate Nucleation. *ACS Sustain. Chem. Eng.* **2017**, *5* (12), 11176−11203.

(17) Thakre, N.; Jana, A. K. Physical and Molecular Insights to Clathrate Hydrate Thermodynamics. *Renew. Sustain. Energy Rev.* **2021**, *135*, 110150.

(18) Malla, B. K.; Chowdhury, S.; Vishwakarma, G.; Kumar, R.; Pradeep, T. Dissociation and Reformation of CO2 Clathrate Hydrate Cages in Amorphous Ice Thin Film under Ultrahigh Vacuum. *J. Phys. Chem. Lett.* **2025**, *16* (20), 4982−4989.

(19) Chowdhury, S.; Malla, B. K.; Vishwakarma, G.; Nyayban, A.; Pradeep, T. Composition-Dependent Formation and Dissociation of Structure I and Structure II Clathrate Hydrates of Trimethylene Oxide in Ultrahigh Vacuum. *J. Phys. Chem. C* **2025**, *129* (19), 8937−8945.

(20) Malla, B. K.; Vishwakarma, G.; Chowdhury, S.; Nayak, S. K.; Yamijala, S. S. R. K. C.; Pradeep, T. Formation and Dissociation of Dimethyl Ether Clathrate Hydrate in Interstellar Ice Mimics. *J. Phys. Chem. C* **2024**, *128* (6), 2463−2470.

(21) Zheng, J.; Chong, Z. R.; Qureshi, M. F.; Linga, P. Carbon Dioxide Sequestration via Gas Hydrates: A Potential Pathway toward Decarbonization. *Energy Fuels* **2020**, *34* (9), 10529−10546.

(22) Fleyfel, F.; Devlin, J. P. Carbon Dioxide Clathrate Hydrate Epitaxial Growth: Spectroscopic Evidence for Formation of the Simple Type-II CO_2 Hydrate. *J. Phys. Chem.* **1991**, *95* (9), 3811−3815.

(23) Bauer, R. P. C.; Ravichandran, A.; Tse, J. S.; Appathurai, N.; King, G.; Moreno, B.; Desgreniers, S.; Sammynaiken, R. In Situ X-Ray Diffraction Study on Hydrate Formation at Low Temperature in a High Vacuum. *J. Phys. Chem. C* **2021**, *125* (48), 26892−26900.

(24) Vishwakarma, G.; Malla, B. K.; Reddy, K. S. S. V. P.; Ghosh, J.; Chowdhury, S.; Yamijala, S. S. R. K. C.; Reddy, S. K.; Kumar, R.; Pradeep, T. Induced Migration of CO_2 from Hydrate Cages to Amorphous Solid Water under Ultrahigh Vacuum and Cryogenic Conditions. *J. Phys. Chem. Lett.* **2023**, *14* (11), 2823−2829.

(25) Devlin, J. P. Structure, Spectra, and Mobility of Low-Pressure Ices: Ice I, Amorphous Solid Water, and Clathrate Hydrates at $T <$ 150 K. *J. Geophys. Res. Planets* **2001**, *106* (E12), 33333−33349.

(26) Vishwakarma, G.; Malla, B. K.; Chowdhury, S.; Khandare, S. P.; Pradeep, T. Existence of Acetaldehyde Clathrate Hydrate and Its

https://doi.org/10.1021/acs.jpclett.6c00029
J. Phys. Chem. Lett. XXXX, XXX, XXX−XXX

Dissociation Leading to Cubic Ice under Ultrahigh Vacuum and Cryogenic Conditions. *J. Phys. Chem. Lett.* **2023**, *14* (23), 5328−5334.
(27) Ghosh, J.; Vishwakarma, G.; Das, S.; Pradeep, T. Facile Crystallization of Ice I h via Formaldehyde Hydrate in Ultrahigh Vacuum under Cryogenic Conditions. *J. Phys. Chem. C* **2021**, *125* (8), 4532−4539.
(28) Ghosh, J.; Bhuin, R. G.; Vishwakarma, G.; Pradeep, T. Formation of Cubic Ice via Clathrate Hydrate, Prepared in Ultrahigh Vacuum under Cryogenic Conditions. *J. Phys. Chem. Lett.* **2020**, *11* (1), 26−32.
(29) Michon, M. A.; Chmielniak, P.; Weber, P. M.; Rose-Petruck, C. Two-Photon Chemistry of Tetrahydrofuran in Clathrate Hydrates. *Phys. Chem. Chem. Phys.* **2024**, *26* (3), 2568−2579.
(30) Ahn, Y. H.; Shin, K.; Lee, J. W. Thermal Expansivity of γ-Irradiated Clathrate Hydrate with Intracavity Conformational Change. *Chem. Phys. Lett.* **2018**, *706*, 14−18.
(31) Ramakrishnan, S.; Sagi, R.; Mahapatra, N.; Asscher, M. Effect of Coadsorbed Oxygen on the Photochemistry of Methane Embedded in Amorphous Solid Water. *J. Phys. Chem. C* **2018**, *122* (27), 15287−15296.
(32) Horowitz, Y.; Asscher, M. Electron-Induced Chemistry of Methyl Chloride Caged within Amorphous Solid Water. *J. Chem. Phys.* **2013**, *139* (15), 154707.
(33) Lilach, Y.; Asscher, M. Photochemistry of Caged Molecules: CD3Cl@Ice. *J. Chem. Phys.* **2003**, *119* (1), 407−412.
(34) Maity, S.; Kaiser, R. I.; Jones, B. M. Formation Of Ketene (H_2CCO) In Interstellar Analogous Methane (CH_4)-Carbon Monoxide (CO) Ices: A Combined Ftir And Reflectron Time-Of-Flight Mass Spectroscopic Study. *Astrophys. J.* **2014**, *789* (1), 36.
(35) Bergantini, A.; Góbi, S.; Abplanalp, M. J.; Kaiser, R. I. A Mechanistical Study on the Formation of Dimethyl Ether (CH3OCH3) and Ethanol (CH3CH2OH) in Methanol-Containing Ices and Implications for the Chemistry of Star-Forming Regions. *Astrophys. J.* **2018**, *852* (2), 70.
(36) Buch, V.; Devlin, J. P.; Monreal, I. A.; Jagoda-Cwiklik, B.; Uras-Aytemiz, N.; Cwiklik, L. Clathrate Hydrates with Hydrogen-Bonding Guests. *Phys. Chem. Chem. Phys.* **2009**, *11* (44), 10245−10265.
(37) Mikuni, H.; Takahasi, M.; Tsuchiya, S. Photolysis of Dimethyl Ether by 184.9 Nm Radiation. *J. Photochem.* **1978**, *9* (4), 481−490.
(38) Schriver, A.; Coanga, J. M.; Schriver-Mazzuoli, L.; Ehrenfreund, P. FTIR Studies of Ultraviolet Photo-Dissociation at 10 K of Dimethyl-Ether in Argon and Nitrogen Matrices, in the Solid Phase and in Amorphous Water Ice. *Chem. Phys. Lett.* **2004**, *386* (4−6), 377−383.
(39) Voronova, K.; Mozaffari Easter, C. M.; Covert, K. J.; Bodi, A.; Hemberger, P.; Sztáray, B. Dissociative Photoionization of Diethyl Ether. *J. Phys. Chem. A* **2015**, *119* (43), 10654−10663.
(40) Ghosh, J.; Vishwakarma, G.; Das, S.; Pradeep, T. Facile Crystallization of Ice I h via Formaldehyde Hydrate in Ultrahigh Vacuum under Cryogenic Conditions. *J. Phys. Chem. C* **2021**, *125* (8), 4532−4539.
(41) Vishwakarma, G.; Malla, B. K.; Kumar, R.; Pradeep, T. Partitioning Photochemically Formed CO_2 into Clathrate Hydrate under Interstellar Conditions. *Phys. Chem. Chem. Phys.* **2024**, *26* (22), 16008−16016.
(42) Kulikov, M. Y.; Feigin, A. M.; Schrems, O. H_2O_2 Photo-production inside H2O and H_2O:O_2 Ices at 20−140 K. *Sci. Rep.* **2019**, *9* (1), 1−9.
(43) Yang, Z.; Doddipatla, S.; He, C.; Goettl, S. J.; Kaiser, R. I.; Jasper, A. W.; Gomes, A. C. R.; Galvão, B. R. L. Can Third-Body Stabilisation of Bimolecular Collision Complexes in Cold Molecular Clouds Happen? *Mol. Phys.* **2024**, *122* (1−2), No. e2134832.
(44) Bulak, M.; Paardekooper, D. M.; Fedoseev, G.; Chuang, K. J.; Terwisscha Van Scheltinga, J.; Eistrup, C.; Linnartz, H. Quantification of O_2 Formation during UV Photolysis of Water Ice: H_2O and H_2O:CO_2 Ices. *Astron. Astrophys.* **2022**, *657*, A120.
(45) De Souza Machado, G.; Martins, E. M.; Baptista, L.; Bauerfeldt, G. F. Prediction of Rate Coefficients for the H_2CO + OH → HCO + H_2O Reaction at Combustion, Atmospheric and Interstellar Medium Conditions. *J. Phys. Chem. A* **2020**, *124* (11), 2309−2317.
(46) Gerakines, P. A.; Moore, M. H.; Hudson, R. L. Carbonic Acid Production in H_2O + CO_2 Ices. UV Photolysis vs. Proton Bombardment Carbonic Acid Production in H_2O:CO_2 Ices UV Photolysis vs. Proton Bombardment. *Astron. Astrophys.* **2000**, *357*, 793−800.
(47) Abplanalp, M. J.; Kaiser, R. I. Implications for Extraterrestrial Hydrocarbon Chemistry: Analysis of Ethylene (C_2H_4) and D4-Ethylene (C_2D_4) Ices Exposed to Ionizing Radiation via Combined Infrared Spectroscopy and Reflectron Time-of-Flight Mass Spectrometry. *Astrophys. J.* **2017**, *836* (2), 195.

https://doi.org/10.1021/acs.jpclett.6c00029
J. Phys. Chem. Lett. XXXX, XXX, XXX−XXX